OCEANOGRAPHY

North Atlantic salinity as a predictor of Sahel rainfall

10.1126/sciadv.1501588

Laifang Li,[1]* Raymond W. Schmitt,[1] Caroline C. Ummenhofer,[1] Kristopher B. Karnauskas[2]

Water evaporating from the ocean sustains precipitation on land. This ocean-to-land moisture transport leaves an imprint on sea surface salinity (SSS). Thus, the question arises of whether variations in SSS can provide insight into terrestrial precipitation. This study provides evidence that springtime SSS in the subtropical North Atlantic ocean can be used as a predictor of terrestrial precipitation during the subsequent summer monsoon in Africa. Specifically, increased springtime SSS in the central to eastern subtropical North Atlantic tends to be followed by above-normal monsoon-season precipitation in the African Sahel. In the spring, high SSS is associated with enhanced moisture flux divergence from the subtropical oceans, which converges over the African Sahel and helps to elevate local soil moisture content. From spring to the summer monsoon season, the initial water cycling signal is preserved, amplified, and manifested in excessive precipitation. According to our analysis of currently available soil moisture data sets, this 3-month delay is attributable to a positive coupling between soil moisture, moisture flux convergence, and precipitation in the Sahel. Because of the physical connection between salinity, ocean-to-land moisture transport, and local soil moisture feedback, seasonal forecasts of Sahel precipitation can be improved by incorporating SSS into prediction models. Thus, expanded monitoring of ocean salinity should contribute to more skillful predictions of precipitation in vulnerable subtropical regions, such as the Sahel.

INTRODUCTION

Terrestrial precipitation heavily relies on moisture evaporating from the ocean surface (*1*–*9*). Indeed, oceanic evaporation is the origin and largest element of the global water cycle, exceeding total river flows by an order of magnitude (*1*, *4*, *5*, *9*) and dominating the freshwater budget at global and regional scales (*3*, *6*, *7*). Furthermore, the water cycle is closely coupled to the global energy balance, in that the latent heat associated with evaporation is the largest energy transfer mechanism (more than 88 W m^{-2}) from ocean to atmosphere to balance the radiative heat flux into the climate system (*10*–*12*). Thus, the ocean-to-land moisture flux has important implications for maintaining the global water and energy balances (*6*).

This moisture exchange process leaves its imprint on the sea surface salinity (SSS) pattern, both spatially and temporally (*4*, *9*, *13*–*23*). Globally, high-SSS regions are located where evaporation exceeds precipitation, that is, a net loss of freshwater from the ocean surface (*1*, *4*, *5*). Over large regions of the subtropics, evaporation can exceed precipitation by 1 to 2 m per year, representing an energy export to other regions of 75 W m^{-2} for every meter per year of net water loss. That is, high-salinity regions are major sources of moisture and latent heat for the rest of the climate system, implying that salinity should be a valuable indicator for understanding variability in the water cycle (*9*, *15*). This provides motivation for investigating the relationship between ocean salinity and terrestrial precipitation.

Previous studies have focused on the "response" of ocean salinity to the water cycle, treating salinity as a passive indicator of local freshwater forcing (*17*–*23*). As the atmosphere serves to bridge the water cycle of the ocean and adjacent land, whether and how salinity can be used as a predictor of terrestrial precipitation are the questions investigated here. This study provides evidence that SSS over the subtropical oceans can serve as a seasonal predictor of terrestrial precipitation, focusing on the subtropical North Atlantic and the African Sahel, where monsoonal precipitation is critically important for human health, agriculture, and socioeconomic stability (*24*).

[1]Physical Oceanography Department, Woods Hole Oceanographic Institution, Woods Hole, MA 02543, USA. [2]Department of Atmospheric and Oceanic Sciences and Cooperative Institute for Research in Environmental Sciences, University of Colorado Boulder, Boulder, CO 80303, USA.
*Corresponding author. Email: lli@whoi.edu

RESULTS

Salinity and Sahel precipitation

To examine the relationship between SSS and precipitation, we applied singular value decomposition (SVD) (*25*) to the covariance matrix of African precipitation and Atlantic SSS anomaly (SSSA) data for the period 1950–2009 (see Materials and Methods). The precipitation data are from the National Oceanic and Atmospheric Administration (NOAA) Precipitation Reconstruction over Land (Prec/L), and the salinity data are from the Hadley Centre EN4.1.1 archive (see Materials and Methods). The SSSA signal leads precipitation by one season, indicating potential predictive skill for terrestrial precipitation over Africa (Fig. 1). Specifically, the leading SVD mode (that is, SVD-1) explains 44% of the variance between springtime [March-April-May (MAM)] SSSA and monsoon-season [June-July-August-September (JJAS)] precipitation over Africa. The significant precipitation signal appears over the Sahel (10°N to 20°N, 20°W to 30°E) (Fig. 1B), and the corresponding SSSA signals are over the subtropical North Atlantic and South Atlantic (Fig. 1A). SVD-1 has stronger loading over the subtropical North Atlantic than its southern hemispheric counterpart (Fig. 1A). Consistent with the spatial distribution of SVD-1, the SSSA and precipitation SVD time series are significantly correlated with SSS in the North Atlantic box ($R = 0.88$) and precipitation in the Sahel box ($R = 0.95$), respectively (Fig. 1C; see Materials and Methods).

The lead relationship between springtime SSSA and African monsoon-season precipitation as shown in SVD-1 can be verified by a cross correlation between African monsoon-season precipitation and SSSA in the subtropical North and South Atlantic (Fig. 2 and figs. S1 to S3, A and B). Consistent with Fig. 1, the most coherent and significant correlation is between springtime North Atlantic SSSA and summertime precipitation

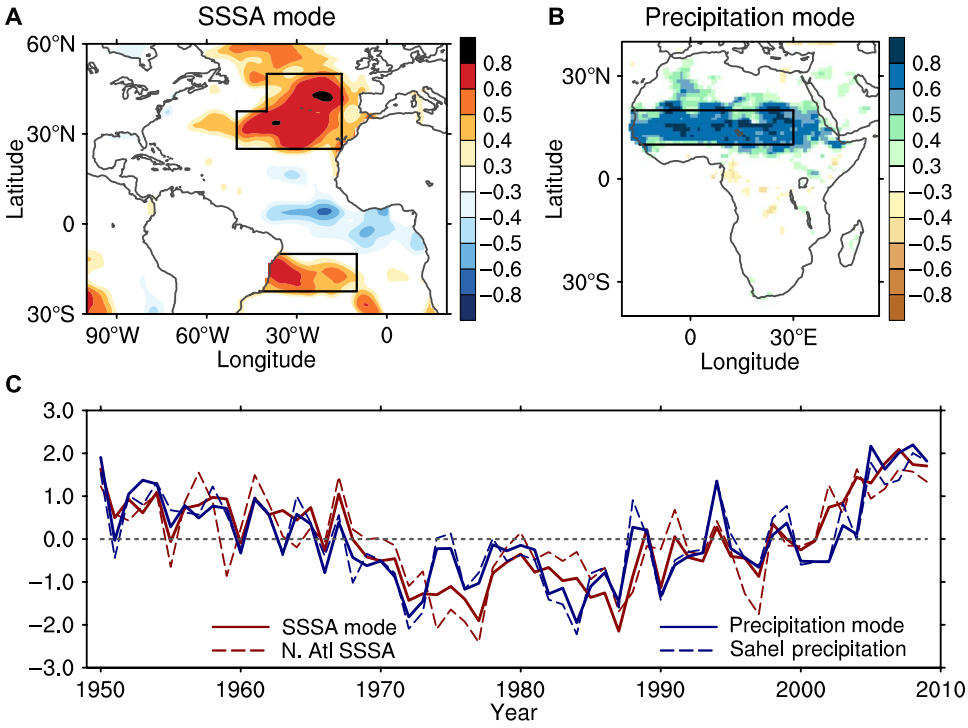

Fig. 1. Springtime Atlantic SSSA and Sahel monsoon-season rainfall. (**A** and **B**) The leading SVD mode of springtime (March to May) Atlantic SSSA (A) and June-to-September African precipitation (B). Shading indicates where the loading of the SVD mode is significant at the $\alpha = 0.05$ level. The North Atlantic and South Atlantic regions are marked on (A), and the box in (B) denotes the Sahel region. (**C**) Time series of the first SVD modes of SSSA (solid red curve) and precipitation (solid blue curve), as well as the normalized March-to-May SSSA in the North Atlantic region (dashed red curve) and June-to-September Sahel precipitation (dashed blue curve).

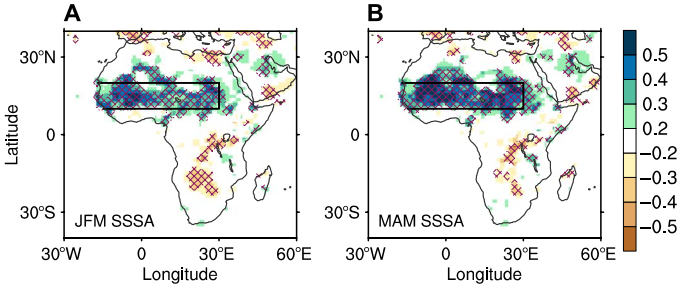

Fig. 2. North Atlantic SSSA leads Sahel precipitation. (**A** and **B**) Correlation between June-to-September African precipitation and (A) wintertime [January-February-March (JFM)] and (B) springtime (MAM) SSSA over the North Atlantic. Areas with correlation coefficients significant at the $\alpha = 0.05$ level are hatched. The effective degrees of freedom used to determine the significance level are calculated using tools described in Materials and Methods.

over the Sahel, with correlation coefficients reaching 0.58 ($P < 0.01$) (Fig. 2B). The South Atlantic SSSA also significantly correlates with Sahel precipitation, albeit with lower correlation coefficients (fig. S3B). In addition, a significant correlation with Sahel precipitation is already emerging in the wintertime (January to March) SSSA (Fig. 2A). These results are robust across data sets (table S1; see the Supplementary Materials for details), which consistently show wintertime and springtime SSSA in the North and South Atlantic leading monsoon-season precipitation in the Sahel (figs. S1 to S3, A and B). Overall, the analysis identifies a significant lead relationship between Atlantic SSSA and monsoon-season precipitation in the Sahel, suggesting that terrestrial precipitation is potentially predictable on the basis of ocean salinity.

Physical processes

With the foregoing evidence that SSS is a strong indicator of the oceanic water cycle and the moisture exchange between ocean and land by atmospheric transport (*3*, *4*, *6*, *7*, *15*), atmospheric moisture budgets were examined to elucidate the processes that physically link ocean salinity and Sahel precipitation.

Composite analysis was used to construct atmospheric moisture flux fields from the National Centers for Environmental Prediction (NCEP)/National Center for Atmospheric Research (NCAR) reanalysis data associated with the high- and low-salinity cases (Fig. 3; see Materials and Methods). In the spring, high salinity in both the North Atlantic and South Atlantic regions is accompanied by strong moisture flux divergence (MFD) away from the local ocean. The increase in MFD indicates that more moisture is leaving the two net moisture export regions in the spring to sustain precipitation elsewhere (Fig. 3A and fig. S3C). Over the subtropical North Atlantic, the increased MFD is maximal in the eastern part of the domain, reaching 0.8 mm day^{-1} (Fig. 3A). In addition, in the subtropical South Atlantic, the increases in MFD are mainly over the southern part of the domain (fig. S3C). In both subtropical regions, the maximum increases in MFD slightly shift from the centers of maximum SSSA, reflecting the contributions of ocean currents in advecting the SSSA forced by surface freshwater flux (*26*, *27*).

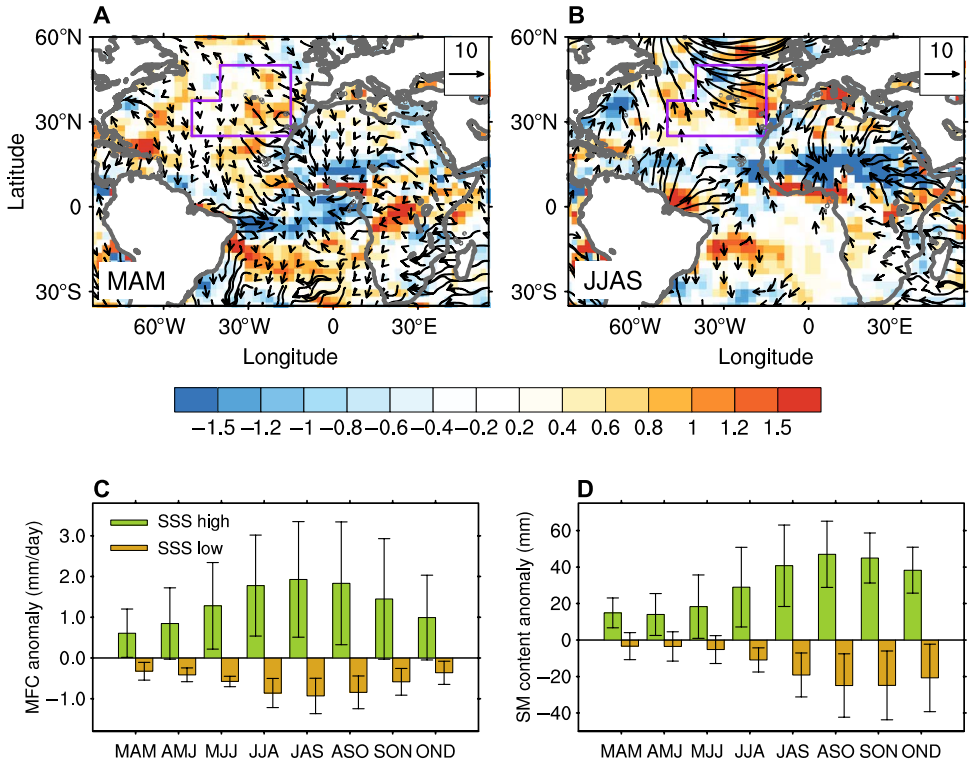

Fig. 3. Mechanisms linking springtime SSSA and Sahel monsoon-season precipitation. (**A** and **B**) Moisture flux divergence anomaly (shaded; mm day^{-1}) and the divergent component of moisture flux (vectors; kg m^{-1} s^{-1}) composites on North Atlantic SSSA: (A) March-to-May composite; (B) June-to-September composite. Vectors are only shown for moisture flux anomalies significant at the 0.05 level according to a Hotelling t^2 test (*65*). The purple boxes denote the subtropical North Atlantic. (**C** and **D**) Moisture flux convergence anomaly (C) and soil moisture (SM) content anomaly (D) over the Sahel composited on springtime North Atlantic SSSA. The green bars are composites of high-SSS events, and the brown bars are those of low-SSS events. The high-SSS events and low-SSS events are selected as the top and bottom decile of the North Atlantic MAM SSS time series. The error bars denote the upper and lower bound of soil moisture or moisture flux convergence (MFC) anomaly defined by 1 SD. AMJ, April-May-June; MJJ, May-June-July; JJA, June-July-August; JAS, July-August-September; ASO, August-September-October; SON, September-October-November; OND, October-November-December.

Analysis of MFD suggests a potential linkage between salinity in the net moisture export regions and terrestrial precipitation. In addition, we calculated the divergent component of the moisture flux to identify regions where moisture export can physically contribute to Sahel precipitation (see Materials and Methods). Examining the divergent component of the moisture flux reveals that the contributions of North and South Atlantic moisture to the variation of Sahel precipitation differ significantly. With positive springtime (MAM) SSSA in the North Atlantic, the increased MFD from the subtropical ocean tends to move toward the Sahel and converge there (Fig. 3A). In contrast, the increased moisture fluxes originating from the South Atlantic are mainly directed poleward rather than toward the Sahel (fig. S3C). Thus, the statistically significant relationship between South Atlantic SSSA and Sahel precipitation is not physically meaningful but must be derived from other teleconnections linking the Northern and Southern Hemisphere expressions of the Hadley circulation (*28*).

The divergent component of moisture flux suggests that the water cycle in the subtropical North Atlantic that generates the SSSA directly contributes to the regional water balance in the African Sahel during the spring season. Accompanying the high SSSA, the local ocean appears to be an additional moisture source that supplies moisture to the African Sahel (*7*). It is noteworthy that in the monsoon season, the increased MFC over the Sahel more likely originates from the tropical eastern Atlantic and the Mediterranean, two climatological moisture source regions identified by previous studies (*7*, *29*–*31*). In contrast, the summer moisture flux over the subtropical North Atlantic tends to diverge toward the midlatitudes (Fig. 3B). The results, however, do not contradict our claim that moisture fluxes over the subtropical North Atlantic can physically influence the monsoon-season precipitation through preconditioning. In the following sections, we will show that the moisture supply from the subtropical North Atlantic provides the initial moisture that can be extended to the subsequent monsoon season through a positive contribution by local soil moisture.

In the Sahel, the moisture flux from remote sources is balanced by the local rate of change of soil moisture content (fig. S4; see the Supplementary Materials for details). Furthermore, previous studies have characterized the Sahel as an area of active land-atmosphere interaction, through which soil moisture couples with atmospheric moisture flux to influence precipitation (*32*–*36*). Figure 3 (C and D) shows the seasonal evolution of atmospheric MFC and soil moisture anomalies during high- and low-salinity years. Consistent with Fig. 3A, in high-salinity years, the moisture flux from the North Atlantic provides an above-normal moisture supply to the Sahel region in spring (Fig. 3C). According to the regional moisture budget analysis, the 0.8–mm day^{-1} increases in net moisture

export from the subtropical North Atlantic during high-salinity years can lead to 1.1–mm day^{-1} increases in MFC in the Sahel because the area of the North Atlantic SSS box (Fig. 1A) is about 40% larger than the Sahel box (Fig. 1B). This expected increase in MFC matches that observed over the Sahel (1 mm day^{-1}) during high-salinity years in comparison with low-salinity years (Fig. 3C). The 1–mm day^{-1} differences in MFC almost triple the MAM climatology of precipitation in the Sahel (0.3 mm day^{-1} according to Prec/L) and are about 80% of the annual mean precipitation in the region. The results suggest that moisture supplied from the subtropical North Atlantic can significantly modulate the springtime regional moisture balance in the Sahel. The increased moisture supply elevates the level of soil moisture content (Fig. 3D) as constrained by the land surface moisture balance (see the Supplementary Materials for details). In the subsequent months, MFC and soil moisture content further increase to peak in the summer monsoon season (Fig. 3, C and D). The seasonal evolution of soil moisture content anomalies in the Sahel is also supported by the composite using a 30-year merged soil moisture product developed in the framework of the European Space Agency's (ESA) Water Cycle Multi-mission Observation Strategy and Climate Change Initiative (CCI) projects, as well as a case study using the 5-year soil moisture record (2010–2014) from the Soil Moisture and Ocean Salinity (SMOS) satellite (figs. S5 and S6; see the Supplementary Materials for details).

The mutual reinforcement of soil moisture anomalies and MFC suggests a positive coupling between soil moisture and atmospheric circulation (*35*, *37*, *38*). Specifically, the wetter soil conditions will moisten the atmospheric boundary layer, destabilize the lower troposphere, and favor the convection and convergence of airflow into the Sahel (Fig. 3B) (*39*). The changes in circulation provide favorable conditions for MFC, which can further moisten the local land surface. At the same time, wet soil can contribute to precipitation by increasing local evaporation (*33*, *40*). According to our analysis, such a positive coupling is stronger in the composites of high SSS cases than in those of low SSS cases (Fig. 3, C and D), which is consistent with previous studies suggesting the dependency of land-atmospheric coupling strength on the wetness of soil (*41*).

We acknowledge the limitations of both model-based and satellite remote sensing soil moisture data sets in our mechanistic studies of the observed salinity-precipitation relationship. However, the consistency between the three independent data sets suggests that a positive contribution of soil moisture can be an important factor to link the springtime salinity signal in the subtropical North Atlantic with summertime Sahel precipitation. We now focus on the rainfall-predictive skill that this newly identified SSS-precipitation relationship provides for the African Sahel.

Predictability of Sahel rainfall using North Atlantic SSSA

The significant relationship between springtime North Atlantic SSSA and Sahel monsoon-season precipitation can help to improve seasonal forecasts of Sahel rainfall, especially because it is found that the SSSA signals are independent of previously identified sea surface temperature anomalies (SSTA) modes (*42*–*50*) (fig. S7; see the Supplementary Materials for details).

Here, we demonstrate the improvements in seasonal forecasts of Sahel precipitation using North Atlantic SSSA as a predictor. Random forest regression/prediction (*51*), a machine-learning algorithm, was applied to assess the predictability of summertime Sahel precipitation (see Materials and Methods). The prediction model ranks the North Atlantic SSSA as the most important predictor among the eight variables (including the seven SSTA-based predictors listed in table S2) incorporated in the random forest algorithm (Fig. 4A). The importance factor of North Atlantic SSSA is 1.16, but it drops to 0.52 for the Pacific Decadal Oscillation (PDO), the second most important predictor (Fig. 4A), indicating that the North Atlantic SSSA, first identified in this study, is overwhelmingly more important than the previously identified SST predictors.

Consequently, incorporating SSSA into the prediction model does improve the seasonal forecast of Sahel monsoon-season precipitation. Specifically, the random forest regression/prediction can achieve a skillful prediction of Sahel monsoon-season precipitation (Fig. 4B). The predicted time series explains 58% of the observed precipitation variance (R^2 = 0.58), and the observed precipitation is within the 95% confidence interval of the prediction (Fig. 4B). The predictive skill, however, would decrease substantially if SSSA were excluded from the prediction model. The prediction without SSSA underestimates the variability of precipitation by about 65%, and the R^2 decreases to 0.22 (Fig. 4C). In contrast, the predictions with SSS alone explain 40% of the observed rainfall variance. Except for the early 1970s and mid-1980s, when the SSSA-based prediction underestimated the drought intensity, the predicted precipitation closely follows the observations (fig. S8A).

In addition, we constructed prediction models using multiple linear regression methods (figs. S9 and S10; see the Supplementary Materials for details). Both methods demonstrate substantial improvements in

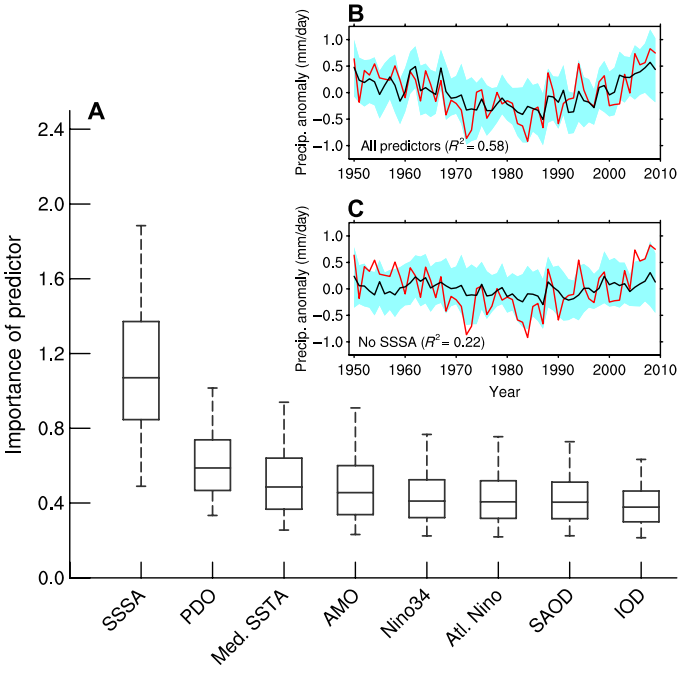

Fig. 4. Sahel rainfall prediction using North Atlantic SSSA. (**A**) Box-and-whisker plot of the importance of predictors for Sahel monsoon-season precipitation according to 1000 trials of the random forest regression. Definition of the importance factor is in the Materials and Methods. Med. SSTA, Mediterranean SSTA; AMO, Atlantic Multidecadal Oscillation; Nino34, Niño 3.4; Atl. Nino, Atlantic Niño; SAOD, South Atlantic Ocean Dipole; IOD, Indian Ocean Dipole. (**B** and **C**) Precipitation anomaly (bold black curves; mm day^{-1}) over the Sahel predicted by the random forest algorithm: (B) prediction using the combination of all predictors including SSSA (Materials and Methods); (C) prediction without the SSSA predictor. The light blue envelope is the 95% confidence interval derived from 1000 trials of the regression. The red curve is the observed precipitation anomaly. The Sahel precipitation predicted by each predictor is shown in fig. S8.

Sahel rainfall prediction with knowledge of the springtime SSSA signal over the subtropical North Atlantic. The random forest regression, which is capable of representing the nonlinear relationship between predictors and response, improves the accuracy of Sahel rainfall prediction over the multiple linear regression model (Fig. 4B and fig. S10A).

Overall, this study suggests that springtime North Atlantic SSSA provides significant skill for predicting monsoon-season precipitation over the Sahel. Thus, in addition to previously identified SSTA modes (*42*, *45*–*47*), incorporating subtropical North Atlantic SSSA can substantially improve the seasonal forecast of Sahel rainfall.

DISCUSSION

SSS reflects the variability and changes of the oceanic water cycle, serving as "nature's rain gauge" (*15*, *22*). Previous research efforts were primarily directed toward understanding the response of salinity to the water cycle (*13*, *14*, *17*, *18*, *20*, *22*, *23*), whereas its potential role as a rainfall predictor has been previously underappreciated. From the perspective of ocean-to-land moisture transport, this study investigated the potential of SSSA as a predictor of terrestrial precipitation. For the first time, the springtime SSSA over the subtropical North Atlantic has been identified as a physically meaningful predictor for Sahel precipitation during the summer monsoon season.

This analysis shows that higher springtime SSS over certain regions of the subtropical North Atlantic tends to be followed by above-normal monsoon-season precipitation over the African Sahel. Physically, the high springtime salinity over the subtropical North Atlantic is associated with enhanced MFD from the local ocean, which is directed toward and converges over the Sahel. This excessive moisture flux from the subtropical oceans elevates local soil moisture content in the Sahel, and the latter, in turn, provides a positive feedback to precipitation through its positive coupling with moisture flux from remote sources. The positive contribution of soil moisture to Sahel regional hydroclimate is one of the likely mechanisms to extend the springtime water cycling signal in the subtropical oceans to the monsoon season. This proposed mechanism is supported by currently available soil moisture data sets from multiple sources, including satellite remote sensing and those derived from water balance models. However, we acknowledge the limitations of these data sets (for example, assumptions made in land-surface water balance model and remote sensing retrieval algorithms) in corroborating the detailed processes involved in the proposed mechanism. Thus, we leave the further discussion of physical mechanisms open and expect that a better understanding of the connection between salinity and terrestrial precipitation will be achieved with more reliable soil moisture data sets.

It is noteworthy that the relationship between North Atlantic SSSA and Sahel precipitation is not merely an imprint of SSTA's influence on precipitation (fig. S7). Thus, the springtime SSSA signal can be used as an independent predictor of Sahel precipitation. The constructed prediction models, both the machine-learning algorithm and the multiple linear regression model, show significantly improved forecasts of Sahel monsoon-season precipitation with the knowledge of springtime SSSA.

Our study provides evidence that SSSA can be a very important predictor of terrestrial precipitation by virtue of it being an integrator of "upstream" water exchanges between oceanic and terrestrial moisture reservoirs. In particular, oceanic regions with evaporation exceeding precipitation and thus higher SSS are exporting moisture (and latent heat energy) to other areas, indicating potential teleconnection patterns between SSSA and the water cycle in other regions. Thus, this study calls further attention to the need for sustained ocean salinity measurements. In this context, it is worth noting that the present generation of satellites that use L-band radiometry [SMOS and Soil Moisture Active Passive (SMAP)] for salinity and soil moisture should prove useful for improved seasonal rainfall predictions in the Sahel.

MATERIALS AND METHODS

Experimental design

To extract a maximum covariance pattern between African monsoon precipitation and pre–monsoon season SSSA over the Atlantic Ocean, we applied SVD analysis (*25*) to the covariance matrix derived from the 60-year JJAS precipitation and MAM SSSA. The leading SVD mode (SVD-1) explains, in total, 44% of the precipitation and SSSA variance (Fig. 1, A and B). The precipitation mode shows the largest loading over the Sahel region (Fig. 1B), whereas the SSSA mode shows two centers of actions: the subtropical North Atlantic and the subtropical South Atlantic (Fig. 1A).

According to the leading SVD mode, we define the Sahel precipitation index as the JJAS precipitation averaged within the box delineated in Fig. 1B. At the same time, the North Atlantic and South Atlantic SSSA indices are respectively defined as the area-averaged SSSA within the two subtropical boxes shown in Fig. 1A. The two-mode time series are highly correlated with the area-averaged SSSA ($R = 0.88$) and Sahel precipitation ($R = 0.95$), respectively. The high correlation coefficients are not merely due to the presence of the low-frequency variability in the time series. After removing the low-frequency quadratic variation from the time series, the correlations remain almost unchanged: $R = 0.76$ ($R = 0.93$) between the area-averaged North Atlantic SSSA (Sahel precipitation) and SSS (precipitation) mode time series (table S3).

To explore the possible physical processes that connect the springtime SSSA signal to monsoon-season precipitation, we applied composite analysis to related variables. The high- and low-salinity cases are the years with SSSA ranked in the top and bottom decile of the salinity index time series. Atmospheric circulation, that is, MFD and the divergent component of moisture flux, was composited during the high/low-SSS cases to quantify the moisture export from the Atlantic and its exchange with the African continent. Linear trends in all data have been removed before analysis, and the study focuses primarily on interannual-interdecadal variability.

With the physical mechanisms diagnosed in the study, we aimed to assess the feasibility of predicting Sahel precipitation using preseason subtropical SSSA. A random forest regression method was applied, taking potential nonlinear relationships between predictors and response into account. The random forest regression is a machine-learning algorithm that takes an ensemble learning approach for prediction. The algorithm is based on the average of decision trees that are built according to input training samples (*51*). The training processes rely on bootstrap aggregating. The algorithm repeatedly subsamples the input data to create regression trees that best fit the relationship between predictors and responses. After training, predictions based on unseen samples can be made by the ensemble from the trained regression trees. According to previous studies, the random forest algorithm has advantages in predictive modeling because of its ability to avoid overfitting (*51*).

In the random forest algorithm, we train the model with eight variables, that is, North Atlantic SSSA and seven SSTA-based predictors identified in previous studies (table S2). The seven SSTA-based predictors are averaged over the MAM months to match the SSSA. The random forest algorithm ranks the importance of predictors in the constructed regression trees. Here, the importance of the *i*th predictor is quantified as the errors that would be introduced to the prediction if the *i*th predictor was permutated while the other predictors remain unchanged.

Using the eight predictors, we constructed a random forest regression model to predict Sahel monsoon-season precipitation. The prediction was run 1000 times. Each time, 30 samples were randomly drawn for training the algorithm, whereas the remaining 30 samples were used for prediction. Combining the eight predictors, the prediction by the random forest regression explains 58% of the observed precipitation variance (Fig. 4B). The observed precipitation is within the 95% confidence interval derived from the 1000 iterations of the prediction (Fig. 4B). Furthermore, we decomposed the prediction skill to the contributions from each individual predictor. Consistent with the importance factors shown in Fig. 4A, North Atlantic SSSA makes the most significant contribution to Sahel rainfall prediction (fig. S8A). The SSSA alone explains 40% of the observed rainfall variance, although the SSSA prediction underestimates the drought intensity during the early 1970s and mid-1980s (fig. S8A). Except for these two periods, the predicted precipitation closely follows the observations (fig. S8A). In contrast, the predictions using SSTA predictors substantially underestimate the interannual variation of Sahel precipitation (fig. S8, B to H); thus, these climate indices are less skillful in predicting the precipitation.

Observational data

Precipitation data sets. The primary precipitation data set used in this study was the NOAA Prec/L. The data cover the period from 1948 until 2015. We used the high-resolution version of the data set (0.5° × 0.5°) at monthly temporal resolution (*52*). To ensure the robustness of the relationship between springtime North Atlantic SSSA and Sahel precipitation, we tested the results in Fig. 2 using four other independent precipitation data sets. These include the Global Historical Climatology Network (*53*, *54*), University of Delaware (*55*), Global Precipitation Climatology Centre (*56*), and Climate Research Unit (*57*) (table S1). These data sets differ in spatial resolution, sources of observational data, and data assimilation/objective analysis methods (table S1).

Figure S1 shows the correlation between pre–monsoon season North Atlantic SSS and African precipitation in JJAS using the four precipitation data sets over the common analysis period of 1950–2009. Consistent with Fig. 2, the significant correlation between springtime North Atlantic SSS and the Sahel monsoon-season precipitation appears in all of the four data sets. Further, the data sets consistently show a stronger springtime signal than in winter (fig. S1). Although the exact correlation coefficient differs among the data sets, likely due to the differences in observational sources, data assimilation methods, and spatial resolution, the key conclusions in Fig. 2 are verified. Thus, the results obtained in this study are robust and independent of precipitation data sets. We used Prec/L for subsequent analysis in the study, and the analysis period was 1950–2009.

Salinity data sets. The salinity data used in this study are from the UK Met Office EN4.1.1 observational data set (*58*). The sources of the observations are mainly from the World Ocean Database 2005 (the global temperature-salinity profile program and the Argo float data). These observed salinity profiles are quality-controlled. We used the objectively analyzed data product, with horizontal resolution of 1° × 1° and monthly temporal resolution. The SSS in this data set refers to salinity measured at 5-m depth.

We also assessed the dependence of the North Atlantic SSSA–Sahel precipitation relationship on the selection of salinity data sets by correlating the North Atlantic SSSA from Simple Ocean Data Assimilation (SODA) 2.2.4 with African monsoon-season precipitation. Consistent with Fig. 1, the springtime SSSA over the subtropical North Atlantic shows the most significant correlation with monsoon-season precipitation over the Sahel (fig. S2). The results, combined with those in fig. S1, suggest that the relationship between North Atlantic SSSA and Sahel precipitation is not sensitive to the choices of available salinity and precipitation data sets. This ensures the robustness of our conclusions built on the observed SSSA-precipitation relationships.

Soil moisture. The soil moisture was adopted from the NOAA Climate Prediction Center (CPC) soil moisture version 2. The data are taken monthly and cover the global terrestrial area with 0.5° × 0.5° resolution (*59*). It is noteworthy that the data are not from observational sources but rather from models constrained by the land surface water balance. However, the data are used because it is the only global soil moisture data set that provides long enough records covering the analysis period.

In addition, we verified our results using the soil moisture data from a 30-year merged soil moisture product developed in the framework of ESA CCI projects (*60*) and SMOS satellite remote sensing products (*61*). The soil moisture composite upon the 30-year ESA CCI soil moisture qualitatively shows the same results as the NOAA CPC data (fig. S5), supporting the conclusions that soil moisture helps to extend the initial moisture flux signal. The results are also supported by the case study based on the short SMOS soil moisture record (2010–2014), that is, that high-salinity years are associated with increased soil moisture in spring over the Sahel, which is further amplified in subsequent months to the monsoon season (fig. S6; see the Supplementary Materials for details).

NCEP/NCAR reanalysis. We used NCEP/NCAR reanalysis data set (*62*) to calculate the processes associated with the atmospheric branch of the water cycle. This data set is generally consistent with others in quantifying the water cycle processes associated with the global monsoon. The moisture flux was calculated as $\frac{1}{g}\int_0^{p_s} q\mathbf{V}\,dp$, where q is specific humidity, V is horizontal wind vector, and p_s is surface pressure. The MFD was thus quantified as $\mathrm{MFD} = \frac{1}{g}\nabla\cdot\int_0^{p_s} q\mathbf{V}\,dp$. The divergent component of the moisture flux was derived on the basis of MFD by solving the Poisson equations (*63*). In Fig. 3 and fig. S3, the units of MFD have been converted to millimeter per day to be consistent with precipitation.

Statistical analysis

Significance test. Here, the cross-correlation coefficients between springtime SSSA and monsoon-season African precipitation were calculated as

$$R = \frac{\sum_{i=1}^{N}(x_i - \bar{x})(y_i - \bar{y})}{\left(\sqrt{\sum_{i=1}^{N}(x_i - \bar{x})^2}\right)\left(\sqrt{\sum_{i=1}^{N}(y_i - \bar{y})^2}\right)}$$

where N is the sample size (60 in this case). The effective degrees of freedom (N^*) were calculated as

$$N^* = \frac{(N-1)\left(1 - r_{xx}(d\tau)r_{yy}(d\tau)\right)}{1 + r_{xx}(d\tau)r_{yy}(d\tau)}$$

taking into account the low-frequency variability presented in both the salinity and precipitation time series (Fig. 1C). Here, $r_{xx}(d\tau)$ and $r_{yy}(d\tau)$

are the lag-1 autocorrelation of North Atlantic SSSA and precipitation, respectively (*64*). In the Sahel, the effective degrees of freedom at each grid cell are in the range of 30 to 35. The significance level of the correlation coefficients was determined on the basis of a Student's t test, in which the t statistics is calculated as $t = \frac{R}{\sqrt{(1-R^2)/(N^*-2)}}$ for a sample with N^* degrees of freedom. It is noteworthy that the definition of N^* is based on the assumption that the time series represent AR(1) processes. Using a partial autocorrelation function, we confirm that both the salinity and precipitation time series generally fulfill the AR(1) assumption. However, we are aware that the limited number of data samples makes it difficult to ascertain that the AR(1) process is stationary. We thus recalculated the correlation coefficients by removing the low-frequency quadratic terms from the original time series (table S3). The obtained significance level is consistent with that derived using N^*.

The Student's t test was also applied to the composite analysis of MFD, whereas the two-sample Hotelling t^2 (*65*) test was applied to determine the significance of the differences in the divergent component of moisture flux during high- and low-SSS years. Specifically, we have a set of two response variables (u and v), which were measured for each of the two cases. Suppose the (u, v) in the high-SSS cases is distributed as two-variable multivariate normal distribution $X \sim N_2(\boldsymbol{u_1}, \Sigma_1)$ with mean vector $\boldsymbol{u_1}$ and covariance matrix Σ_1. At the same time, (u, v) in the low-SSS case has the distribution $Y \sim N_2(\boldsymbol{u_2}, \Sigma_2)$. The null hypothesis is $\boldsymbol{u_1} = \boldsymbol{u_2}$, meaning that the divergent component of moisture flux does not differ between the high- and low-SSS cases. The null hypothesis can be tested using the t^2 statistics

$$t^2 = \frac{n_x n_y}{n_x + n_y}(\bar{x} - \bar{y})^T W^{-1}(\bar{x} - \bar{y})$$

which has the T^2 distribution, that is

$$t^2 \sim T^2(2, n_x + n_y - 2)$$

Here, n_x and n_y are the number of high-SSS and low-SSS cases, respectively, and are set to 6 in this study

$$\bar{x} = \frac{1}{n_x}\sum_{i=1}^{n_x} x_i$$

$$\bar{y} = \frac{1}{n_y}\sum_{i=1}^{n_y} y_i$$

and W^{-1} is the inverse matrix of W, which is calculated as

$$W = \frac{1}{n_x + n_y - 2}\left(\sum_{i=1}^{n_x}(x_i - \bar{x})(x_i - \bar{x})^T + \sum_{i=1}^{n_x}(y_i - \bar{y})(y_i - \bar{y})^T\right)$$

The null hypothesis can be rejected at α significance level if $t^2 > T^2_{1-\alpha,\, 2, n_x+n_y-2}$.

Goodness-of-fit test. The performance of rainfall predictions was evaluated on the basis of the coefficient of determination

$$R^2 = 1 - \frac{\mathrm{SS_{res}}}{\mathrm{SS_{tot}}}$$

$$\mathrm{SS_{tot}} = \sum_{i=1}^{N}(y - \bar{y})^2$$

quantifies the total variance of observed precipitation

$$\mathrm{SS_{res}} = \sum_{i=1}^{N}\left(f(X)_i - y_i\right)^2$$

is the sum of variance unexplained by the prediction model, where $f(X)$ is the random forest prediction. In the multiple linear regression model, the R^2 defined above equates to the square of the correlation coefficients between predictions and observations.

SUPPLEMENTARY MATERIALS

Supplementary material for this article is available at http://advances.sciencemag.org/cgi/content/full/2/5/e1501588/DC1

Supplementary Materials and Methods

fig. S1. SSSA-Sahel rainfall relationship independent of precipitation data sets.

fig. S2. Evaluation of SSSA-Sahel rainfall relationship using salinity.

fig. S3. Relationship between South Atlantic SSSA and Sahel precipitation.

fig. S4. Land surface moisture balance in the Sahel.

fig. S5. Consistency of soil moisture feedback mechanism as shown by NOAA CPC and ESA CCI products.

fig. S6. North Atlantic SSSA–Sahel precipitation mechanism verified by remote sensing (SMOS) soil moisture data.

fig. S7. SSSA-rainfall relationship independent of SSTA.

fig. S8. Random forest regression using eight predictors.

fig. S9. Linear model selection to predict Sahel monsoon-season precipitation.

fig. S10. Linear model prediction of Sahel monsoon-season precipitation.

table S1. Four precipitation data sets used in this study.

table S2. SSTA-based predictors used to construct the random forest regression model for Sahel monsoon-season precipitation.

table S3. Pairwise cross correlation between SSS mode, precipitation mode, North Atlantic MAM salinity, and Sahel JJAS precipitation.

References (*66–80*)

REFERENCES AND NOTES

1. R. W. Schmitt, The ocean component of the global water cycle. *Rev. Geophys.* **33**, 1395–1409 (1995).
2. K. E. Trenberth, Atmospheric moisture recycling: Role of advection and local evaporation. *J. Climate* **12**, 1368–1381 (1999).
3. L. Gimeno, A. Drumond, R. Nieto, R. M. Trigo, A. Stohl, On the origin of continental precipitation. *Geophys. Res. Lett.* **37**, L13804 (2010).
4. G. Lagerloef, R. Schimitt, J. Schanze, H.-Y. Kao, The ocean and the global water cycle. *Oceanography* **23**, 82–93 (2010).
5. J. J. Schanze, R. W. Schmitt, L. L. Yu, The global oceanic freshwater cycle: A state-of-the-art quantification. *J. Mar. Res.* **68**, 569–595 (2010).
6. K. E. Trenberth, J. T. Fasullo, J. Mackaro, Atmospheric moisture transports from ocean to land and global energy flows in reanalyses. *J. Climate* **24**, 4907–4924 (2011).
7. L. Gimeno, A. Stohl, R. M. Trigo, F. Dominguez, K. Yoshimura, L. Yu, A. Drumond, A. M. Durán-Quesasa, R. Nieto, Oceanic and terrestrial sources of continental precipitation. *Rev. Geophys.* **50**, RG4003 (2012).
8. M. Rodell, H. K. Beaudoing, T. S. L'Ecuyer, W. S. Olson, J. S. Famiglietti, P. R. Houser, R. Adler, M. G. Bosilovich, C. A. Clayson, D. Chambers, E. Clark, E. J. Fetzer, X. Gao, G. Gu, K. Hilburn, G. J. Huffman, D. P. Lettenmaier, W. T. Liu, F. R. Robertson, C. A. Schlosser, J. Sheffield, E. F. Wood, The observed state of the water cycle in the early twenty-first century. *J. Climate* **28**, 8289–8318 (2015).
9. P. J. Durack, Ocean salinity and the global water cycle. *Oceanography* **28**, 20–31 (2015).
10. K. E. Trenberth, J. T. Fasullo, J. Kiehl, Earth's global energy budget. *Bull. Am. Meteorol. Soc.* **90**, 311–323 (2009).
11. G. L. Stephens, J. Li, M. Wild, C. A. Clayson, N. Loeb, S. Kato, T. L'Ecuyer, P. W. Stackhouse Jr., M. Lebsock, T. Andrews, An update on Earth's energy balance in light of the latest global observations. *Nat. Geosci.* **5**, 691–696 (2012).
12. T. S. L'Ecuyer, H. K. Beaudoing, M. Rodell, W. Olson, B. Lin, S. Kato, C. A. Clayson, E. Wood, J. Sheffield, R. Adler, G. Huffman, M. Bosilovich, G. Gu, F. Robertson, P. R. Houser, D. Chambers, J. S. Famiglietti, E. Fetzer, W. T. Liu, X. Gao, C. A. Schlosser, E. Clark, D. P. Lettenmaier, K. Hilbur, The observed state of the energy budget in the early twenty-first century. *J. Climate* **28**, 8319–8346 (2015).

13. R. B. Curry, B. Dickson, I. Yashayaev, A changes in the freshwater balance of the Atlantic Ocean over the past four decades. *Nature* **426**, 826–829 (2003).
14. T. P. Boyer, S. Levitus, J. I. Antonov, R. A. Locarnini, H. E. Garcia, Linear trends in salinity for the World Ocean, 1955–1998. *Geophys. Res. Lett.* **32**, L01604 (2005).
15. R. W. Schmitt, Salinity and the global water cycle. *Oceanography* **21**, 12–19 (2008).
16. P. A. Stott, R. T. Sutton, D. M. Smith, Detection and attribution of Atlantic salinity changes. *Geophys. Res. Lett.* **35**, L21702 (2008).
17. S. Hosoda, T. Suga, N. Shikama, K. Mizuno, Global surface layer salinity change detected by Argo and its implication for hydrological cycle intensification. *J. Oceanogr.* **65**, 579–596 (2009).
18. K. P. Helm, N. L. Bindoff, J. A. Church, Changes in the global hydrological-cycle inferred from ocean salinity. *Geophys. Res. Lett.* **37**, L18701 (2010).
19. P. J. Durack, S. E. Wijffels, Fifty-year trends in global ocean salinities and their relationship to broad-scale warming. *J. Climate* **23**, 4342–4436 (2010).
20. P. J. Durack, S. E. Wijffels, R. J. Matear, Ocean salinities reveal strong global water cycle intensification during 1950 to 2000. *Science* **336**, 455–458 (2012).
21. D. W. Pierce, P. J. Gleckler, T. P. Barnett, B. D. Santer, P. J. Durack, The fingerprint of human-induced changes in the ocean's salinity and temperature fields. *Geophys. Res. Lett.* **39**, L21704 (2012).
22. L. Terray, L. Corre, S. Cravatte, T. Delcroix, G. Reverdin, A. Ribes, Near-surface salinity as nature's rain gauge to detect human influence on the tropical water cycle. *J. Climate* **25**, 958–977 (2012).
23. N. Skliris, R. Marsh, S. A. Josey, S. A. Good, C. Liu, R. P. Allan, Salinity changes in the world ocean since 1950 in relation to changing surface freshwater fluxes. *Clim. Dynam.* **43**, 709–736 (2014).
24. I. Niang, I. O. C. Ruppel, M. A. Abdrabo, A. Essel, C. Lennard, J. Padgham, P. Urquhart, *Africa, In Climate Change 2014: Impacts, Adaptation, and Vulnerability. Part B: Regional Aspects. Contribution of Working Group II to the Fifth Assessment Report of the Intergovernmental Panel on Climate Change*, V. R. Barros, C. B. Field, D. J. Dokken, M. D. Mastrandrea, K. J. Mach, T. E. Bilir, M. Chatterjee, K. L. Ebi, Y. O. Estrada, R. C. Geniva, B. Girma, E. S. Kissel, A. N. Levy, S. MacCraken, P. R. Mastrandea, L. L. White, Eds. (Cambridge Univ. Press, Cambridge, UK and New York, 2014), pp. 1199–1265.
25. C. S. Bretherton, C. Smith, J. M. Wallace, An intercomparison of methods for finding coupled patterns in climate data. *J. Climate* **5**, 541–560 (1992).
26. L. Yu, A global relationship between the ocean water cycle and near-surface salinity. *J. Geophys. Res.-Oceans* **116**, C10025 (2011).
27. A. L. Gordon, C. F. Giulivi, Ocean eddy freshwater flux convergence into the North Atlantic subtropics. *J. Geophys. Res.* **119**, 3327–3335 (2014).
28. P. Ceppi, Y.-T. Hwang, X. Liu, D. M. W. Frierson, D. L. Hartmann, The relationship between the ITCZ and the Southern Hemispheric eddy-driven jet. *J. Geophys. Res.-Atmos.* **118**, 5136–5146 (2013).
29. D. L. Cadet, N. O. Nnoli, Water vapour transport over Africa and the Atlantic Ocean during summer 1979. *Q. J. Roy. Meteorol. Soc.* **113**, 581–602 (1987).
30. B. Fontaine, P. Roucou, S. Trzaska, Atmospheric water cycle and moisture fluxes in the West African monsoon: Mean annual cycles and relationship using NCEP/NCAR reanalysis. *Geophys. Res. Lett.* **30**, 1117 (2003).
31. W. T. Liu, X. Xie, K. B. Katsaros, Observation of oceanic origin of Sahel precipitation from space. *Remote Sens. Environ.* **123**, 593–599 (2012).
32. J. G. Charney, Dynamics of deserts and drought in the Sahel. *Q. J. Roy. Meteorol. Soc.* **101**, 193–202 (1975).
33. C. Gong, E. Eltahir, Sources of moisture for rainfall in West Africa. *Water Resour. Res.* **32**, 3115–3121 (1996).
34. N. Zeng, J. D. Neelin, K.-M. Lau, C. J. Tucker, Enhancement of interdecadal climate variability in the Sahel by vegetation interaction. *Science* **286**, 1537–1540 (1999).
35. R. D. Koster, P. A. Dirmeyer, Z. Guo, G. Bonan, E. Chan, P. Cox, C. T. Gordon, S. Kanae, E. Kowalczyk, D. Lawrence, P. Liu, C.-H. Lu, S. Malyshev, B. McAvaney, K. Mitchell, D. Mocko, T. Oki, K. Oleson, A. Pitman, Y. C. Sud, C. M. Taylor, D. Verseghy, R. Vasic, Y. Xue, T. Yamada, Regions of strong coupling between soil moisture and precipitation. *Science* **305**, 1138–1140 (2004).
36. C. M. Taylor, A. Gounou, F. Guichard, P. P. Harris, R. J. Ellis, F. Couvreux, M. De Kauwe, Frequency of Sahelian storm initiation enhanced over mesoscale soil-moisture patterns. *Nat. Geosci.* **4**, 430–433 (2011).
37. H. Douville, F. Chauvin, Relevance of soil moisture for seasonal climate predictions: A preliminary study. *Clim. Dynam.* **16**, 719–736 (2000).
38. P. A. Dirmeyer, C. A. Schlosser, K. L. Brubaker, Precipitation, recycling, and land memory: An integrated analysis. *J. Hydrometeorol.* **10**, 278–288 (2009).
39. S. M. Hagos, K. H. Cook, Dynamics of the West African monsoon jump. *J. Climate* **20**, 5264–5284 (2007).
40. A. Berg, B. R. Lintner, K. Findell, S. I. Seneviratne, B. van den Hurk, A. Ducharne, F. Chéruy, S. Hagemann, D. M. Lawrence, S. Malyshev, A. Meierk, P. Gentine, Interannual coupling between summertime surface temperature and precipitation over land: Processes and implications for climate change. *J. Climate* **28**, 1308–1328 (2015).
41. Z. Guo, P. A. Dirmeyer, Interannual variability of land–atmosphere coupling strength. *J. Hydrometeorol.* **14**, 1636–1646 (2013).
42. J. Bader, M. Latif, The impact of decadal-scale Indian Ocean sea surface temperature anomalies on Sahelian rainfall and the North Atlantic Oscillation. *Geophys. Res. Lett.* **30**, 2169 (2003).
43. C. K. Folland, T. N. Palmer, D. E. Parker, Sahel rainfall and worldwide sea temperatures, 1901–85. *Nature* **320**, 602–607 (1986).
44. A. Giannini, R. Saravanan, P. Chang, Oceanic forcing of Sahel rainfall on interannual to interdecadal time scales. *Science* **302**, 1027–1030 (2003).
45. S. Janicot, S. Trzaska, I. Poccard, Summer Sahel-ENSO teleconnection and decadal time scale SST variations. *Clim. Dynam.* **18**, 303–320 (2001).
46. T. M. Shanahan, J. T. Overpeck, K. J. Anchukaitis, J. W. Beck, J. E. Cole, D. L. Dettman, J. A. Peck, C. A. Scholz, J. W. King, Atlantic forcing of persistent drought in West Africa. *Science* **324**, 377–380 (2009).
47. B. Rodríguez-Fonseca, E. Mohino, C. R. Mechoso, C. Caminade, M. Biasutti, M. Gaetani, J. Garcia-Serrano, E. K. Vizy, K. Cook, Y. Xue, I. Polo, T. Losada, L. Druyan, B. Fontaine, J. Bader, F. J. Doblas-Reyes, L. Goddard, S. Janicot, A. Arribas, W. Lau, A. Colman, M. Vellinga, D. P. Rowell, F. Kucharski, A. Voldoire, Variability and predictability of West African droughts: A review of the role of sea surface temperature anomalies. *J. Climate* **28**, 4034–4060 (2015).
48. I. M. Held, T. L. Delworth, J. Lu, K. L. Findell, T. R. Knutson, Simulation of Sahel drought in the 20th and 21st centuries. *Proc. Natl. Acad. Sci. U.S.A.* **102**, 17891–17896 (2005).
49. H. S. Badr, B. F. Zaitchik, S. D. Guikema, Application of statistical models to the prediction of seasonal rainfall anomalies over the Sahel. *J. Appl. Meteorol. Clim.* **53**, 614–636 (2014).
50. Z. T. Segele, M. B. Richman, L. M. Leslie, P. J. Lamb, Seasonal-to-interannual variability of Ethiopia/Horn of Africa monsoon. Part II: Statistical multi-model ensemble rainfall predictions. *J. Climate* **28**, 3511–3536 (2015).
51. L. Breiman, Random forests. *Mach. Learn.* **45**, 5–32 (2001).
52. M. Chen, P. Xie, J. E. Janowiak, P. A. Arkin, Global land precipitation: A 50-yr monthly analysis based on gauge observations. *J. Hydrometeorol.* **3**, 249–266 (2002).
53. T. C. Peterson, R. S. Vose, An overview of the global historical climatology network temperature data base. *Bull. Am. Meteorol. Soc.* **78**, 2837–2849 (1997).
54. P. D. Jones, A. Moberg, Hemispheric and large-scale surface air temperature variations: An extensive revision and an update to 2001. *J. Climate* **16**, 206–223 (2003).
55. C. J. Willmott, K. Matsuura, "Terrestrial air temperature and precipitation: Monthly and annual time series (1950–1999)," 2001; http://climate.geog.udel.edu/~climate/html_pages/README.ghcn_ts2.html.
56. U. Schneider, A. Becker, P. Finger, A. Meyer-Christofer, M. Ziese, B. Rudolf, GPCC's new land surface precipitation climatology based on quality-controlled in situ data and its role in quantifying the global water cycle. *Theor. Appl. Climatol.* **115**, 15–40 (2013).
57. I. Harris, P. D. Jones, T. J. Osborn, D. H. Lister, Updated high-resolution grids of monthly climatic observations—The CRU TS3.10 dataset. *Int. J. Climatol.* **34**, 623–642 (2014).
58. S. A. Good, M. J. Martin, N. A. Rayner, EN4: Quality controlled ocean temperature and salinity profiles and monthly objective analyses with uncertainty estimates. *J. Geophys. Res.-Ocean* **118**, 6704–6716 (2013).
59. H. van den Dool, J. Huang, Y. Fan, Performance and analysis of the constructed analogue method applied to U.S. soil moisture over 1981–2001. *J. Geophys. Res.-Atmos.* **108**, 861 (2003).
60. Y. Y. Liu, R. M. Parinussa, W. A. Dorigo, R. A. M. De Jeu, W. Wagner, A. I. J. M. van Dijk, M. F. McCabe, J. P. Evans, Developing an improved soil moisture dataset by blending passive and active microwave satellite-based retrievals. *Hydrol. Earth Syst. Sci.* **15**, 425–436 (2011).
61. Y. H. Kerr, P. Waldteufel, J. P. Wigneron, J. Font, M. Berger, Soil moisture retrieval from space: The Soil Moisture and Ocean Salinity (SMOS) mission. *IEEE T. Geosci. Remote* **39**, 1729–1735 (2001).
62. E. Kalnay, M. Kanamitsu, R. Kistler, W. Collins, D. Deaven, L. Gandin, M. Iredell, S. Saha, G. White, J. Woollen, Y. Zhu, A. Leetmaa, R. Reynolds, M. Chelliah, W. Ebisuzaki, W. Higgins, J. Janowiak, K. C. Mo, C. Ropelewski, J. Wang, Roy Jenne, Dennis Joseph, The NCEP-NCAR 40-year reanalysis project. *Bull. Am. Meteorol. Soc.* **77**, 437–471 (1996).
63. P. Lynch, Deducing the wind from vorticity and divergence. *Mon. Weather Rev.* **116**, 86–93 (1988).
64. C. S. Bretherton, M. Widmann, V. P. Dymnikov, J. M. Wallace, I. Bladé, The effective number of spatial degrees of freedom of a time-varying field. *J. Climate* **12**, 1990–2009 (1999).
65. H. Hoetlling, The generalization of Student's ratio. *Ann. Math. Statist.* **2**, 360–378 (1931).
66. K. L. Brubaker, D. Entekhabi, P. S. Eagleson, Estimation of continental precipitation recycling. *J. Climate* **6**, 1077–1089 (1993).
67. T. M. Smith, R. W. Reynolds, T. C. Peterson, J. Lawrimore, Improvements to NOAA's historical merged land–ocean surface temperature analysis (1880–2006). *J. Climate* **21**, 2283–2296 (2008).
68. Y. Gouriou, T. Delcroix, Seasonal and ENSO variations of sea surface salinity and temperature in the South Pacific Convergence Zone during 1976–2000. *J. Geophys. Res.-Ocean* **107**, 8011 (2002).

69. G. Grunseich, B. Subrahmanyam, V. S. N. Murty, B. S. Giese, Sea surface salinity variability during the Indian Ocean Dipole and ENSO events in the tropical Indian Ocean. *J. Geophys, Res.-Ocean* **116**, C11013 (2011).
70. J. Mignot, C. Frankignoul, On the interannual variability of sea surface salinity in the Atlantic. *Clim. Dynam.* **20**, 555–565 (2003).
71. C. L. Mallows, Some comments on C_P. *Technometrics* **15**, 661–675 (1973).
72. S. G. Gilmour, The interpretation of Mallows's C_p-statistic. *J. Roy. Stat. Soc. D-Sta.* **45**, 49–56 (1996).
73. R. Zhang, T. L. Delworth, Impact of Atlantic multidecadal oscillations on India/Sahel rainfall and Atlantic hurricanes. *Geophys. Res. Lett.* **33**, L17712 (2006).
74. B. Fontaine, S. Janicot, Sea surface temperature fields associated with West African rainfall anomaly types. *J. Climate* **9**, 2935–2940 (1996).
75. J. Lu, T. L. Delworth, Oceanic forcing of the late 20th century Sahel drought. *Geophys. Res. Lett.* **32**, L22706 (2005).
76. D. P. Rowell, The impact of Mediterranean SSTs on the Sahelian rainfall season. *J. Climate* **16**, 849–862 (2003).
77. D. P. Rowell, Teleconnections between the tropical Pacific and the Sahel. *Q. J. Roy. Meteor. Soc.* **127**, 1683–1706 (2001).
78. C. Caminade, L. Terray, Twentieth century Sahel rainfall variability as simulated by the ARPEGE AGCM, and future changes. *Clim. Dynam.* **35**, 75–94 (2010).
79. H. C. Nnamchi, J. Li, Influence of the South Atlantic Ocean dipole on West African summer precipitation. *J. Climate* **24**, 1184–1197 (2011).
80. Z. Wu, N. E. Huang, Ensemble empirical mode decomposition: A noise-assisted data analysis method. *Adv. Adapt. Data Anal.* **1**, 1–41 (2009).

Acknowledgments: We thank K. Brink, Y. Kushnir, Y.-O. Kwon, A. Miller, C. Wunsch, and A. Solow for helpful discussions; J. Schanze who performed preliminary work on this topic; two anonymous reviewers and Editor C. Garrett for their insightful comments on the manuscript. **Funding:** L.L. is supported by the Postdoctoral Scholar Program at the Woods Hole Oceanographic Institution (WHOI), with funding provided by the Ocean and Climate Change Institute (OCCI). R.W.S. is supported by NASA grants NNX12AF59G and NNX14AH38G and NSF grant OCE-1129646. C.C.U. is supported by NSF grant AGS-1355339. K.B.K. is supported by the Alfred P. Sloan Foundation and the James E. and Barbara V. Moltz Fellowship administered by the WHOI OCCI. **Author contributions:** L.L. performed the analysis and prepared Figs. 1 to 4 and the Supplementary figures. R.W.S. conceived the study. All authors wrote and discussed the manuscript. **Competing interests:** The authors declare that they have no competing interests. **Data and materials availability:** All data needed to obtain the conclusions in the paper are presented in the paper and/or the Supplementary Materials. Additional data related to this paper may be requested from the authors.

Submitted 5 November 2015
Accepted 29 March 2016
Published 6 May 2016
10.1126/sciadv.1501588

Citation: L. Li, R. W. Schmitt, C. C. Ummenhofer, K. B. Karnauskas, North Atlantic salinity as a predictor of Sahel rainfall. *Sci. Adv.* **2**, e1501588 (2016).

ScienceAdvances
AAAS

North Atlantic salinity as a predictor of Sahel rainfall
Laifang Li, Raymond W. Schmitt, Caroline C. Ummenhofer and Kristopher B. Karnauskas (May 6, 2016)
Sci Adv 2016, 2:.
doi: 10.1126/sciadv.1501588